PHYSICAL REVIEW B **84**, 075477 (2011)

Microscopic theory of photonic one-way edge mode

Kejie Fang
Department of Physics, Stanford University, Stanford, California 94305, USA

Zongfu Yu and Shanhui Fan
Department of Electrical Engineering, Stanford University, Stanford, California 94305, USA

(Received 10 May 2011; revised manuscript received 28 July 2011; published 15 August 2011)

We consider a system consisting of a honeycomb lattice of magneto-optical resonators. We show that this system can be very well described by a tight-binding model. Moreover, when truncated, this system supports a one-way edge mode. We discuss the microscopic physics, linking the properties of the one-way edge modes to the corresponding bulk modes.

DOI: 10.1103/PhysRevB.84.075477 PACS number(s): 42.70.Qs, 42.25.Gy

I. INTRODUCTION

Unusual wave propagation effects can occur in systems with broken time-reversal symmetry. In a two-dimensional electron gas, for example, time-reversal symmetry can be broken by a perpendicular static magnetic field. As a result, the system can exhibit a quantum Hall effect, with a unidirectional flow of electrons on the edge of the system.[1–4] Analogous one-way modes of photons have recently been proposed using surface plasmon polaritons,[5] photonic crystals,[6–10] and the interface of two magneto-optical materials.[11] In all cases, time-reversal symmetry is broken by the use of materials exhibiting magneto-optical effects. Most recently, such a one-way edge mode in a photonic crystal has been experimentally observed.[12–14]

In a magneto-optical photonic crystal system,[15–17] the existence of a one-way edge mode is typically linked to a nonzero Chern's number of bulk band structure.[6–8] Such a link is important because it provides a general condition for designing the magneto-optical photonic crystal structure. However, since the Chern's number is a universal number characterizing the topological properties of the band over the entire first Brillouin zone, the microscopic connection, between the properties of the bulk mode and the properties of the one-way edge mode, is not evident in the Chern's number analysis.

In this paper, we consider a model system consisting of a honeycomb lattice of magneto-optical resonators. We show that the existence and the detailed physical properties of the one-way edge modes in this system can be understood in terms of the properties of the bulk modes at the edge of the bulk photonic band gap. This understanding then provides insights into the design of many properties of one-way edge modes.

The paper is organized as follows: in Sec. II we describe our physical model consisting of a honeycomb lattice of resonators, and we present numerical results of the band structure and the eigenmode field distribution at the band edges for this system. In Sec. III we construct a tight-binding model to analytically calculate the band structure of such a honeycomb lattice of resonators. We obtain excellent agreement between the tight-binding model and the numerical results. In Sec. IV, we present a microscopic picture of the emergence of the one-way edge modes in this system, combining the numerical and the tight-binding analyses outlined in the previous sections. In Sec. V, we apply the microscopic picture developed in Sec. IV to other kind of edges, and we design a one-way edge state with a small group velocity.

II. PHYSICAL MODEL

In this section, we introduce the physical model step by step. We start from a photonic crystal with a triangular lattice of air holes in a background with dielectric constant $\epsilon_b = 16$. The lattice constant of the triangular lattice is a and the radius of the air holes is $r = 0.35a$ [Fig. 1(a)]. Figure 1(b) shows the band structure, as calculated using the MIT Photonic-Bands (MPB) package,[18] of transverse electric (TE) modes, which have electric fields that are entirely in-plane. The TE modes have a complete band gap between the frequencies of $0.192(2\pi c/a)$ and $0.295(2\pi c/a)$.

Next we create localized resonance in this band gap. To create a single resonator, we replace one air hole with a rod of magneto-optical material having a radius $r' = 0.5a$ [Fig. 2(a)]. The permittivity tensor of the magneto-optic material has the form

$$\epsilon = \begin{pmatrix} \epsilon_r & -i\epsilon_{\mathrm{i}} & 0 \\ i\epsilon_{\mathrm{i}} & \epsilon_r & 0 \\ 0 & 0 & \epsilon_r \end{pmatrix}, \tag{1}$$

when the magnetization is along the z direction parallel to the rod. We take $\epsilon_r = 16$. Without magnetization, i.e.,$\epsilon_i = 0$, the resonator supports two degenerate dipole-like resonances [Figs. 2(b) and 2(c)] with a frequency $\omega_0 = 0.224(2\pi c/a)$.

We construct a honeycomb lattice of such resonators with a lattice constant $a' = 6a$ [Fig. 3(a)]. A schematic view of the honeycomb lattice, with the two sublattices A and B labeled, as well as the corresponding first Brillouin zone in wave vector space, is shown in Fig. 3(b). Such a lattice supports four photonic bands within the band gap of the photonic crystal [Fig. 3(c)]. A more detailed view of these four bands is shown in Fig. 4(a). The middle two bands touch at K and K', forming two Dirac cones.

In the presence of magnetization ($\epsilon_{\mathrm{i}} \neq 0$), time-reversal symmetry is broken. The individual resonator in Fig. 2 supports two counter-rotating states at different frequencies.[19] For the honeycomb lattice of such resonators, the degeneracy at the K

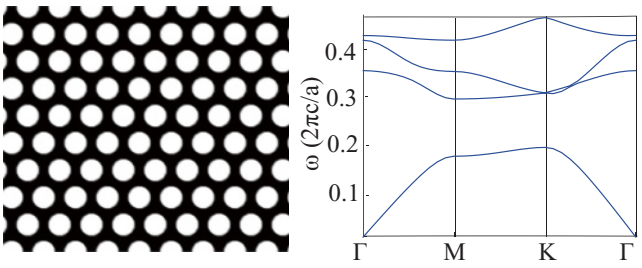

(a) (b)

FIG. 1. (Color online) (a) Photonic crystal consisting of a triangular lattice of air holes introduced in a background material with a dielectric constant $\epsilon_b = 16$. The holes have a radius $r = 0.35a$, where a is the lattice constant. (b) Transverse electric band structure of this photonic crystal.

and K' points is lifted [Fig. 4(b)]. This paper will be entirely concerned with the edge and defect states that are introduced into such a lattice of resonators. For this purpose, we refer to a perfect lattice of such resonators as the "bulk" for the rest of the paper.

III. TIGHT-BINDING MODEL

In this section we will build a tight-binding model to study the bulk band structure as formed by the honeycomb array of localized resonances shown in Fig. 3(a). As shown in Fig. 3(b), every unit cell of the honeycomb lattice contains two nonequivalent sites A and B. At each site there are two different states as shown in Fig. 2(b). As a result, the basis for our tight-binding model contains four states: $|p_x^A\rangle$, $|p_y^A\rangle$, $|p_x^B\rangle$, and $|p_y^B\rangle$. Since the resonance is highly localized, we only consider two interactions: the on-site coupling and the nearest-neighbor coupling. The on-site coupling describes the interaction of two resonances on the same site. For example, for the state $|p_x^A\rangle$ on site A, the on-site interaction is its coupling with $|p_y^A\rangle$ on the same site A. The on-site interaction vanishes when there is no magnetization, i.e., $\epsilon_i = 0$. In the presence of magnetization, the on-site interaction iV_p can be calculated as[19]

$$iV_p = \frac{i}{2}\frac{\omega_0 \int dS \epsilon_i \hat{z} \cdot (\vec{E}_{p_x}^* \times \vec{E}_{p_y})}{\sqrt{\int dS \epsilon_r |\vec{E}_{p_x}|^2 \int dS \epsilon_r |\vec{E}_{p_y}|^2}}, \tag{2}$$

where $\omega_0 = 0.224(2\pi c/a)$ is the frequency of the resonance in the absence of magnetization. $\vec{E}_{p_x}$ and $\vec{E}_{p_y}$ are the electric field of $|p_x\rangle$ and $|p_y\rangle$ states, respectively, dS is an infinitesimal area, and the integration is defined in the unit cell. The nearest-neighbor coupling represents the interaction between two nearest A and B sites and it is generally nonzero. For state $|p_x^A\rangle$ on site A, the nearest-neighbor coupling is its interaction with both $|p_x^B\rangle$ and $|p_y^B\rangle$ on the three nearest B sites surrounding such a site A. For the coupling between the two nearest-neighbor sites with the vector connecting them being along the x direction, we use V_σ to represent the interaction between $|p_x^A\rangle$ and $|p_x^B\rangle$, and V_π to represent the interaction between $|p_y^A\rangle$ and $|p_y^B\rangle$. In this model, the time-reversal-symmetry breaking arises purely from the on-site interaction iV_p. Both V_σ and V_π are assumed to be real, and thus there is no time-reversal-symmetry breaking associated with the nearest-neighbor coupling.

Based on the descriptions above regarding various interactions, and following the standard procedure,[20] we obtain the tight-binding Hamiltonian in momentum space in the basis of $(|p_x^A\rangle, |p_y^A\rangle, |p_x^B\rangle, |p_y^B\rangle)^T$:

$$H = \begin{pmatrix} \omega_0 & iV_p & \left(\frac{3}{2}V_\sigma + \frac{1}{2}V_\pi\right)\cos(3ak_x)e^{i\sqrt{3}ak_y} + V_\pi e^{-i2\sqrt{3}ak_y} & i\frac{\sqrt{3}}{2}(V_\sigma - V_\pi)\sin(3ak_x)e^{i\sqrt{3}ak_y} \\ & \omega_0 & i\frac{\sqrt{3}}{2}(V_\sigma - V_\pi)\sin(3ak_x)e^{i\sqrt{3}ak_y} & \left(\frac{3}{2}V_\pi + \frac{1}{2}V_\sigma\right)\cos(3ak_x)e^{i\sqrt{3}ak_y} + V_\sigma e^{-i2\sqrt{3}ak_y} \\ & & \omega_0 & iV_p \\ & & & \omega_0 \end{pmatrix}, \tag{3}$$

Here we show only the diagonal and the upper half of the Hamiltonian matrix. The lower half of the matrix can be easily obtained since H is Hermitian.

We can obtain the band structure by solving the Hamiltonian in Eq. (3), which can then be compared to the band structure calculated from MPB. This process allows us to fit the coupling coefficient in Eq. (3):

$$V_\sigma = -0.001185, \quad V_\pi = 0.000085 \tag{4}$$

for the case with time-reversal symmetry and

$$V_\sigma = -0.001192, \quad V_\pi = 0.000092, \quad V_p = 0.0007 \tag{5}$$

for the the case where the time-reversal symmetry is broken. All these coupling constants have the unit of angular frequency $2\pi c/a$. Note that the value of coupling constant V_p here corresponds to $\epsilon_i = 1$. We see in Fig. 4 that the tight-binding model reproduces the band structure well, for the cases both with and without magnetization.

Using the tight-binding model, for the band structure shown in Fig. 4(b), we can calculate the Chern's number C_n for the nth band,[4]

$$C_n = \frac{1}{2\pi}\int dk_x \int dk_y \left(\frac{\partial a_y^n(\vec{k})}{\partial k_x} - \frac{\partial a_x^n(\vec{k})}{\partial k_y}\right), \tag{6}$$

where $a_{x,y}^n(\vec{k}) = -i\langle n\vec{k}|\partial_{k_{x,y}}|n\vec{k}\rangle$ is the Berry's gauge field and the integrand is the Berry's curvature, with $\vec{k}$ the Bloch wave vector. $|n\vec{k}\rangle$ is a four-element vector representing an eigenstate

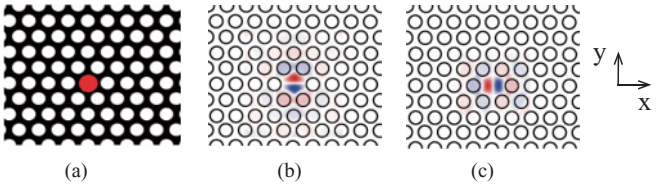

FIG. 2. (Color online) (a) A single resonator introduced into the photonic crystal shown in Fig. 1(a). The resonator consists of a dielectric rod (red) made from magneto-optic material of radius $r' = 0.5a$. (b) and (c) Two dipole modes associated with the resonator. Red and blue correspond to, respectively, large positive and negative out-of-plane magnetic fields.

of the Hamiltonian shown in Eq. (3). We can easily verify that for the first and fourth bands, respectively,

$$C = \pm \mathrm{sgn}(V_p), \tag{7}$$

and for the second and third bands $C = 0$. We see that C is nonzero for the first and fourth bands when $V_p \neq 0$.

Having considered the bulk lattice consisting of an infinite honeycomb array of magneto-optical resonators, we now construct edge modes by truncating the bulk lattice. We consider the structure shown in Fig. 5(b), consisting of an infinite photonic crystal. Half of the crystal consists of a semi-infinite array of a honeycomb lattice of resonators. The other half is a perfect crystal without any resonator. The honeycomb lattice is truncated such that the edge is of a zig-zag type. As seen in the projected band structure of Fig. 5(a), which plots the frequency of all the modes in the system as a function of wave vector k parallel to the edge, such an edge supports a one-way mode in the frequency range between the second and the third bands of the bulk lattice. The field profile of the edge mode at wave vector $k = 0$ is plotted in Fig. 5(b). The field is localized on the outer sites of the zig-zag edge.[21]

IV. THE CONNECTION BETWEEN BULK AND EDGE STATES IN TERMS OF MICROSCOPIC PHYSICS

In the previous section, we have presented a model system with its bulk band structure characterized by a nontrivial topological feature in terms of a nonzero Chern's number, and we demonstrated the existence of one-way edge modes when such a bulk system is truncated. The general connection between the topological feature of the bulk band structure and

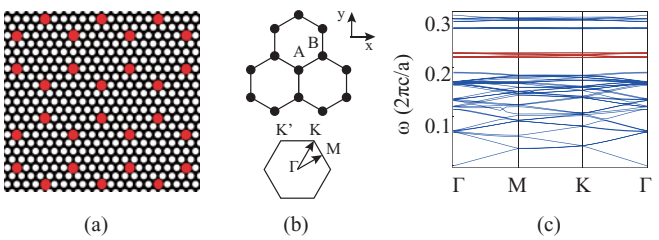

FIG. 3. (Color online) (a) A honeycomb lattice of resonators introduced into the photonic crystal shown in Fig. 1(a). (b) Honeycomb lattice and its first Brillouin zone. (c) TE band structure when $\epsilon_i = 0$. Notice the four bands (red lines) lying in the band gap of the photonic crystals. These four bands are associated with the honeycomb lattice of resonators.

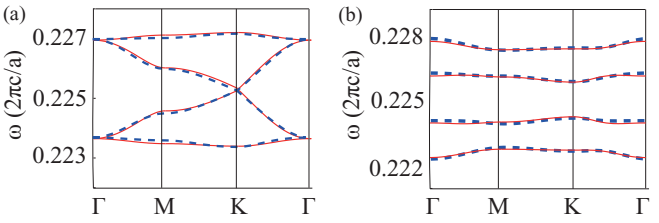

FIG. 4. (Color online) Comparison between band structures calculated using the tight-binding model of Eq. (3) (red solid line) and using MPB (blue dashed line), for the honeycomb lattice of resonators shown in Fig. 3(a). (a) $\epsilon_i = 0$. (b) $\epsilon_i = 1$.

the existence of one-way edge modes is quite well known.[22,23] Such a general conclusion, however, is rather mathematical. Instead, here we aim at establishing the connection between the bulk band structure and various properties of one-way edge modes based on microscopic physics. We will do so by means of first-principles band structure calculations and the tight-binding model.

In the analysis of photonic crystals, it is well known that the properties of defect states can be understood from the bulk state at the edge of the photonic band gap.[24] Here, we show that the property of the edge modes can be understood in terms of the properties of the bulk modes at the K and K' points. In the rest of the paper, we will only consider the band of the edge mode in the bulk band gap between the second and third bands, and the other branches of the edge mode band can be viewed as a continuous extension of this one.

We start by analyzing the field distribution of the second and third bands at the K and K' points in the presence of magnetization, as shown in Fig. 6. At the K point, the field of the second-band mode is localized in sublattice A and rotates clockwise, represented at each A site by $\frac{1}{\sqrt{2}}(|p_x^A\rangle + i|p_y^A\rangle)$, and the field of the third-band mode is localized in sublattice B and rotates counterclockwise, represented at each B site by $\frac{1}{\sqrt{2}}(|p_x^B\rangle - i|p_y^B\rangle)$. On the other hand, at the K' point, the field of the second-band mode is localized in sublattice B and rotates

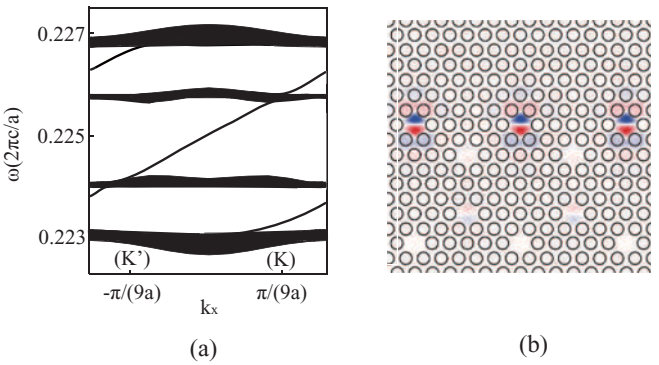

FIG. 5. (Color online) (a) MPB calculation of the projected band structure of a truncated honeycomb lattice with one zig-zag edge. There is a one-way edge mode in the bulk band gap due time-reversal-symmetry breaking. (b) Edge mode field profile corresponding to $k = 0$. The field is highly localized in the magneto-optical rods. In this figure, small circles are air rods and the sites without small circles are magneto-optic rods.

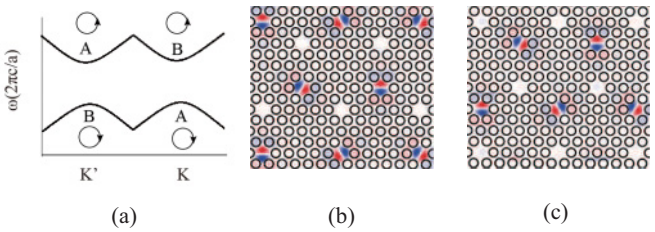

FIG. 6. (Color online) (a) The schematic plot of the field distribution of the second-band and third-band modes of the honeycomb lattice at the K and K' points. Circles with an arrow represent the rotation direction of the fields. Real-space field distribution of (b) third-band mode and (c) second-band mode at the K point.

clockwise, represented at each B site by $\frac{1}{\sqrt{2}}(|p_x^B\rangle + i|p_y^B\rangle)$, and the field of the third-band mode is localized in sublattice A and rotates counterclockwise, represented at each A site by $\frac{1}{\sqrt{2}}(|p_x^A\rangle - i|p_y^A\rangle)$. We note that a time-reversal operation relates the field distributions of the second-band mode at K and the third-band mode at K'. These two modes having different frequencies thus directly indicates time-reversal-symmetry breaking.

Examining Fig. 5, we note that the edge of the truncated bulk lattice lies entirely on the B site. As a result, among the four bulk modes at the K and K' points as discussed above, one expects that the second-band mode at K', and the third-band mode at K, should play a significant role in the formation of the one-way edge mode in this structure, since these modes have most of their energy concentrated at the B site as shown in Fig. 6. In Fig. 5, the edge mode indeed has a band structure that connects the lower bulk gap edge at K' to the upper gap edge at K.

As a more explicit demonstration of the connection between the bulk and the edge, we consider the "spin" of both the bulk and the edge states. The edge modes, as well as the second-band bulk modes near K' and the third-band bulk modes near K, all have most of their fields concentrated on the B sites. For such a mode with a wave vector $\vec{k}$, the field at each B site is $f_x(\vec{k})|p_x^B\rangle + f_y(\vec{k})|p_y^B\rangle$, where $f_x(\vec{k})$ and $f_y(\vec{k})$ are complex numbers satisfying $|f_x(\vec{k})|^2 + |f_y(\vec{k})|^2 = 1$. In the following, we refer to such a modal field on the B site as the "spin" of the photon state, since the field resides in a two-dimensional Hilbert space $\mathcal{H}$ spanned by the two orthogonal basis functions $|p_x^B\rangle$ and $|p_y^B\rangle$.

As a simple way to quantify the "spin," we calculate the expectation value of the operator

$$\sigma = \begin{pmatrix} 0 & -i \\ i & 0 \end{pmatrix}, \tag{8}$$

which acts on a state in the Hilbert space $\mathcal{H}$. The second-band mode at K', which is a clockwise rotating state having $f_x(\vec{k}) = \frac{1}{\sqrt{2}}$ and $f_y(\vec{k}) = \frac{i}{\sqrt{2}}$, has $\langle\sigma\rangle = +1$. The third-band mode at K, which is a counterclockwise rotating state having $f_x(\vec{k}) = \frac{1}{\sqrt{2}}$ and $f_y(\vec{k}) = -\frac{i}{\sqrt{2}}$, has $\langle\sigma\rangle = -1$.

For the edge mode, we plot its $\langle\sigma\rangle$ as a function of wave vector in Fig. 7. We indeed see that the modes having their parallel wave vector corresponding to the projection of K and K' have the same $\langle\sigma\rangle$, and hence the same rotation direction of the fields, as the corresponding bulk modes at K and K'.

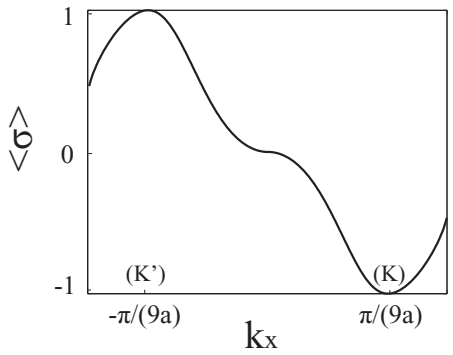

FIG. 7. "Spin" $\langle\sigma\rangle$ of a photon for the edge mode as a function of wave vector. $+1$ (-1) indicates clockwise (counterclockwise) rotating mode with equal weight on $|p_x^B\rangle$ and $|p_y^B\rangle$.

We also study the field distribution of modes in the second and third bands near the K and K' points. Graphically, we represent the state $f_x(\vec{k})|p_x^B\rangle + f_y(\vec{k})|p_y^B\rangle$ by plotting out a parametrized curve $[x(s), y(s)]$, where $x(s) = \mathrm{Re}(f_x(\vec{k})e^{is})$ and $y(s) = \mathrm{Re}(f_y(\vec{k})e^{is})$. Using such a representation, we plot in Fig. 8 the spin of the photon modes in the third band, at a frequency of $\omega = 0.22572(2\pi c/a)$ that is slightly above the third band edge at K. At this frequency, the constant-frequency contour features a closed loop in the wave vector space. We

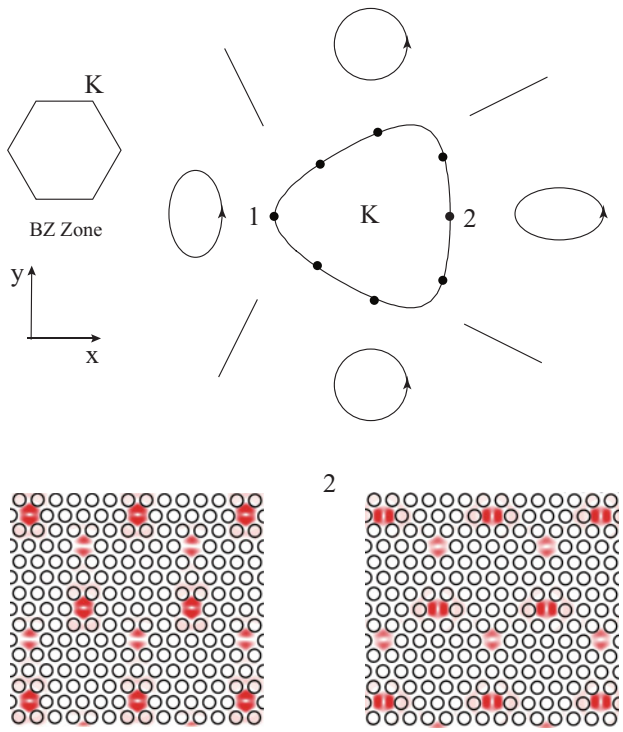

FIG. 8. (Color online) Spin of the bulk modes of the third band at eight k points in momentum space on the constant frequency contour $\omega = 0.22572(2\pi c/a)$ around K. The ratio between the major and minor axes of the ellipse indicates the ratio between $|p_x^B\rangle$ and $|p_y^B\rangle$ components of the mode. The bottom panels show the time-averaged field density of modes at 1 and 2, respectively.

note that the photon spin changes as the wave vector is varied along the contour. At $\vec{k} = (0.042, 0.096)2\pi/a$ (point 1 on the contour in Fig. 8), the state has a larger component in $|p_y^B\rangle$ and the relative phase between $|p_x^B\rangle$ and $|p_y^B\rangle$ is $\frac{\pi}{2}$, and thus the parametrized curve is an ellipse with its major and minor axes parallel to the y axis and x axis, respectively. As a result, the intensity of the mode is more extended along the y direction. On the other hand, at $\vec{k} = (0.065, 0.096)2\pi/a$ (point 2 on the contour in Fig. 8), the state has a larger component in $|p_x^B\rangle$ and the intensity of the mode is less extended along the y direction. Such a wave vector dependency of the photon spin is a direct manifestation of the local Berry's curvature. The Berry's phase γ accumulated along the contour can be expressed as the following equation:

$$\gamma = -\oint |f_y(\vec{k})|^2 \nabla_{\vec{k}} \mathrm{Arg}\left[\frac{f_x(\vec{k})}{f_y(\vec{k})}\right] \cdot d\vec{k} (\mathrm{mod} 2\pi). \qquad (9)$$

The difference in field spatial distribution for the bulk states near K and K' points determines the dispersion slope of the band of the one-way edge mode. For the zig-zag edge along x direction as shown in Fig. 5, the wave vector k_x parallel to the x direction is a conserved quantity. Thus, we can compare the properties of the edge modes at a particular k_x to the corresponding bulk modes with the same k_x. Examining Fig. 8, we see that the two third-band modes 1 and 2, which have their parallel wave vector symmetric with respect to K, have substantially different modal field distributions. Since the truncation is imposed perpendicular to the y direction, the two modes which have their field distribution extending in the y direction in different ways, therefore, will be affected differently. Specifically, in the tight-binding model, the zig-zag edge is characterized by missing bonds in the y direction. As a result, mode 1, which has most of its field aligned with the missing band, will be more strongly affected, and lies deeper inside the gap as compared to mode 2. Thus, the band of the one-way edge mode emerges to the left of point K. The Berry's curvature around the K point for the bulk modes directly determines the slope of the edge modes around the K point. A similar argument can be made for the slope of the edge band around the K' point as well.

V. OTHER KINDS OF EDGE STATES

In the previous sections, using the example of a zig-zag edge of a honeycomb lattice, we have shown that many properties of the one-way edge modes can be understood in terms of the properties of the corresponding bulk modes. Building upon this understanding, here we examine a few other kinds of edges and relate the properties of the edge modes in terms of bulk modes.

In the previous sections, we have also established a close agreement between the tight-binding model and the numerical simulation using MPB. Here, in this section, we will therefore only use the tight-binding model, as described in Sec. III.

As a first example, we consider a truncation of the honeycomb lattice with the same orientation as the zig-zag edge; i.e., the truncation is perpendicular to the y direction, but with the sites on the edge that are on the A site, as shown in Fig. 9. In this case, the edge mode emerges from the second band at K and the third band at K', since at these points the bulk states have most of their fields concentrated on A sites.

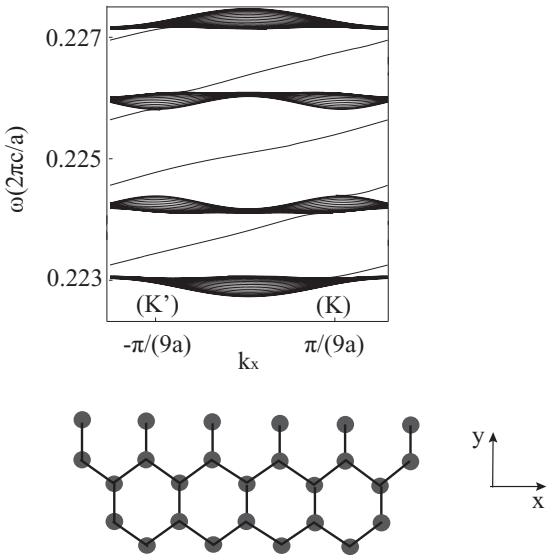

FIG. 9. The band structure of the bulk lattice with an edge missing zig-zag type bonds, as shown in the bottom of the figure. A one-way edge mode emerges from the right-hand side of the$K$ point in the band gap of the second and third bands.

Similar to the analysis for the zig-zag edge, here we also consider the second-band bulk modes near K as shown in Fig. 10. Comparing Fig. 10 to Fig. 8, we see that the second-band bulk modes near K are instead concentrated on the A site and also have their photon spin rotation direction flipped. In this case, the truncation in Fig. 9 will affect mode 2 more significantly, since the missing bands are now predominantly along the x direction. As a result, we see that the one-way edge mode indeed emerges to the right of the K point at the bulk band edge of the second band.

As a second and final example, we show that the detailed property of the one-way edge modes can be tuned by changing the dielectric properties on the edge. Here we again consider the zig-zag edge as shown in Fig. 5, but we set the on-site

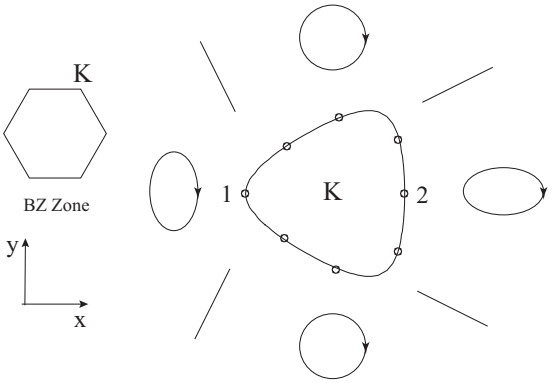

FIG. 10. Spin of the bulk modes of the second band at eight k points in momentum space on the constant frequency contour $\omega = 0.22428(2\pi c/a)$ around K.

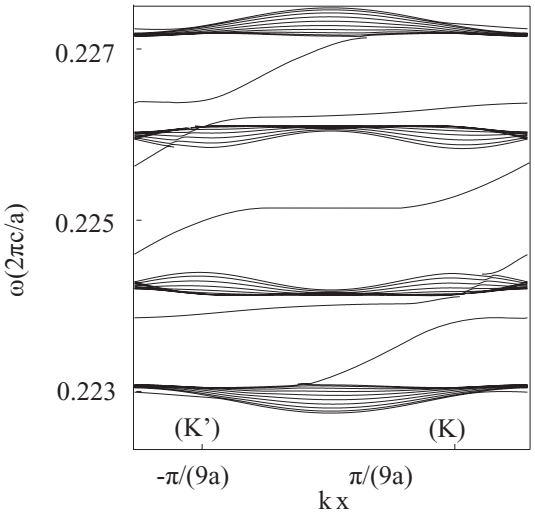

FIG. 11. Slow light. By reducing ϵ_i of the edge, the edge mode dispersion curve in the second band gap near $k = 0$ becomes flat. In this figure we set $V_p = -0.0003$ on one edge.

coupling $V_p = -0.0003$ on the zig-zag edge, which can be accomplished by reducing the on-site magneto-optical coupling only on the edge. In doing so, the band structure of the one-way edge mode now features a flat region near $k_x = 0$, where the group velocity is greatly reduced Fig. 11.[25] Moreover, the group velocity can be tuned by adjusting the on-site coupling strength on the edge, allowing dynamic modulation of such one-way slow light, which is potentially useful for overcoming the delay-bandwidth product constraint in standard static slow-light systems.[26,27]

VI. CONCLUSION AND DISCUSSION

In summary, we have proposed a system consisting of a honeycomb lattice of magneto-optical resonators, which supports one-way edge modes when truncated. We showed that the properties of this system can be well described by a tight-binding model, which greatly facilitates analytic understanding of the one-way edge modes.

Using a combination of a tight-binding model and a first-principles band structure calculation on this system, we have provided a discussion of the connection between the properties of the bulk and the edge modes. Our analysis complements the usual Chern's number analysis of this system, by emphasizing the microscopic physics of bulk-edge connection.

For demonstration purposes, we have chosen a large magneto-optical parameter, as well as a dilute honeycomb lattice of resonators, where a tight-binding model can be applied. However, the general conclusions regarding the connection between bulk and edge states that we discussed here should be applicable to other magneto-optical photonic crystal systems. In particular, we showed that the existence of Berry's curvature results in a strong $\vec{k}$ dependency of the spatial distribution of the bulk modes. When the edge is introduced, these different bulk modes are then affected differently, giving rise to a local slope of the edge modes in the vicinity of the bulk band edge. We also showed that the global aspects of the edge modes across the entire first Brillouin zone can be traced to different bulk band edge modes localized on different sublattices of the system. These results may have general applicability for magneto-optical photonic crystals exhibiting one-way edge modes, since the conditions here are directly related to the topological aspects of the bulk band structure, which is robust with respect to significant parameters and structural variations.

[1] K. v. Klitzing, G. Dorda, and M. Pepper, Phys. Rev. Lett. **45**, 494 (1980).
[2] R. B. Laughlin, Phys. Rev. B **23**, 5632 (1981).
[3] B. I. Halperin, Phys. Rev. B **25**, 2185 (1982).
[4] D. J. Thouless, M. Kohmoto, M. P. Nightingale, and M. den Nijs, Phys. Rev. Lett. **49**, 405 (1982).
[5] Z. Yu, G. Veronis, Z. Wang, and S. Fan, Phys. Rev. Lett. **100**, 023902 (2008).
[6] S. Raghu and F. D. M. Haldane, Phys. Rev. A **78**, 033834 (2008).
[7] F. D. M. Haldane and S. Raghu, Phys. Rev. Lett. **100**, 013904 (2008).
[8] Z. Wang, Y. D. Chong, J. D. Joannopoulos, and M. Soljacic, Phys. Rev. Lett. **100**, 013905 (2008).
[9] X. Ao, Z. Lin, and C. T. Chan, Phys. Rev. B **80**, 033105 (2009).
[10] T. Ochiai and M. Onoda, Phys. Rev. B **80**, 155103 (2009).
[11] H. Zhu and C. Jiang, Opt. Express **18**, 6914 (2010).
[12] Z. Wang, Y. Chong, J. D. Joannopoulos, and M. Soljacic, Nature (London) **461**, 772 (2009).
[13] J. X. Fu, R. J. Liu, and Z. Y. Li, Appl. Phys. Lett. **97**, 041112 (2010).
[14] Y. Poo, R. X. Wu, Z. Lin, Y. Yang, and C. T. Chan, Phys. Rev. Lett. **106**, 093903 (2011).
[15] A. Figotin and I. Vitebsky, Phys. Rev. E **63**, 066609 (2001).
[16] M. Inoue *et al.*, J. Phys. D **39**, R151 (2006).
[17] A. Khanikaev and M. Steel, Photonics Nanostructures **8**, 125 (2010).
[18] S. Johnson and J. Joannopoulos, Opt. Express **8**, 173 (2001).
[19] Z. Wang and S. Fan, Appl. Phys. B **81**, 369 (2005).
[20] G. Grosso and G. Parravicini, *Solid State Physics* (Academic, New York, 2000), Chap. V, p. 145.
[21] In both the MPB and the tight-binding model calculation, we have used a bulk lattice with a finite thickness, which therefore has two edges. The thickness of the bulk lattice is chosen to be large enough such that the two edges do not couple. In the plots, we show only modes that are confined to one of the two edges.
[22] Y. Hatsugai, Phys. Rev. Lett. **71**, 3697 (1993).
[23] Y. Hatsugai, Phys. Rev. B **48**, 11851 (1993).
[24] J. Joannopoulos *et al.*, *Photonic Crystal-Molding the Flow of Fight* (Princeton University Press, Princeton, NJ, 2008), Chap. 5, p. 78.
[25] A different design of a one-way slow-light waveguide was recently considered in C. Huang and C. Jiang, J. Opt. Soc. Am. B **26**, 1954 (2009).
[26] M. F. Yanik and S. Fan, Phys. Rev. Lett. **92**, 083901 (2004).
[27] M. F. Yanik, W. Suh, Z. Wang, and S. Fan, Phys. Rev. Lett. **93**, 233903 (2004).